RoboBoat 2021: Technical Design Report Barunastra ITS Roboboat Team

Sitorus A, Alhakim A, Setiaji M, Rahman F, Ramadhan C, El-Hasan Z, Akbar A, Permatasari F, Hakim M, Tana V, Siraj F, Medina Q, Indaryo A, Fadhlurrahman M, Ramadhan R, Aditya N, Solang D, Atmaja H, Kautaman G, Prawoto M, Damayanti Z, Sundana P, Farhan A, Dikairono R.
Institut Teknologi Sepuluh Nopember
Surabaya, Indonesia
barunastra.its@gmail.com

***Abstract*—To compete in International Roboboat Competition (IRC) 2021, Barunastra ITS proposed Nala Poseidon, the new Autonomous Surface Vehicle (ASV) design. This ASV is an improvement of the previous ASV that have competed in IRC 2019. Small-Waterplane-Area Twin-Hull is introduced to be the new ASV hull type for its characteristics that decrease motion response caused by waves. This hull ensures better vision sensor reading due to decreased camera vertical movements affected by disturbed flow downstream. To perform algorithm testing and data gathering, Gazebo simulator and MATLAB were used. The ASV software architecture used Robot Operating System as its backbone to ensure code maintainability. The computer vision was made more efficient and constantly maintained its robustness. The new LiDAR Segmentation System was presented as the ASV vision extension to obtain the objects' distance relative to LiDAR. This additional information leads to a better ASV perception. Improved Guided Navigation Control also contributes to better global control navigation, producing 50% less error over the desired path. Hydrophone array was used to locate active pinger location with an improved Time Difference of Arrival method.**

Keyword—ASV, Small-Waterplane-Area Twin-Hull, Computer Vision, Global Navigation Control, Acoustic Signal Processing

I. COMPETITION STRATEGY

Each year, Barunastra ITS consistently conducts technology advancement in order to carry on its core vision. The team successfully passed 3 out of 5 missions conducted in International Roboboat Competition (IRC) 2019's final run. Therefore, to cater to such performance this year, the team focuses on formulating a harmony of technologies that would help the Autonomous Surface Vehicle (ASV) complete the missions given in IRC 2021. This section of Competition Strategy will further discuss Barunastra's unique approach to complete each mission.

A. Mandatory Navigation Channel

The Mandatory Navigation Channel comes up as the first mission that must be completed. The ASV must perform autonomous navigation to pass through two sets of gates consisting of a pair of red and green Sur-Mark buoys [1].

To perform this mission, the ASV would approach the Mandatory Navigation Channel using the navigation system until the pair of Sur-Mark buoys are detected. The ASV then would move forward while maintaining the ASV heading to the middle point between the Sur-Mark buoys.

B. Speed Gate

The second mission ASV would attempt is the Speed Gate. This mission requires full throttle thrust and good maneuverability. Therefore, it is logical to put this mission to be the second mission as the ASV's battery is still plentifully charged. This plan is executed to achieve a high time point. The camera is utilized for local control. After gaining perspective of the ASV's surroundings, the ASV proceeds to detect two gate buoys before surging through the buoys' middle point until they are no longer in the ASV's perception. With its

local control, the ASV detects the targeted blue buoy, proceeding to approach it. The ASV will attempt to circumnavigate around the blue buoy afterward. The circumnavigation will be done until the initial gate buoys come to the ASV's perception. Then, it begins to exit the Speed Gate arena through the gate buoys.

C. Obstacle Channel

In this mission, the ASV is expected to find a way to maneuver through a defined path made of buoys while avoiding any contact with them [1]. Initially, the ASV's local control is availed to detect and recognize features such as, in this case, barrier buoys. Consequently, when the ASV encounters an obstacle buoy, it would look for the nearest sufficient gap to move through.

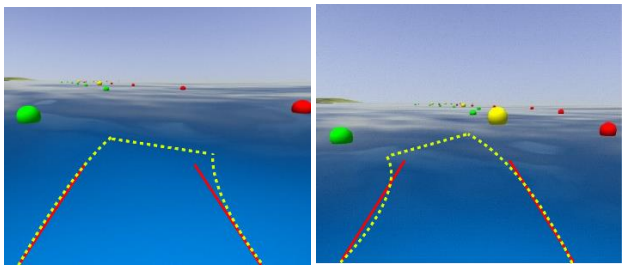

Fig. 1. Obstacle Channel Illustration. Red for ASV Front Area, Yellow for Steering

Hence, ASV needs good maneuverability to excel in this task. Other than algorithm optimization, the ASV is also equipped with upgraded mechanical components. Two mechanical components are highlighted. The first one is the hull, which is designed based on Small-Waterplane-Area Twin-Hull (SWATH) type hull. The second one is the thruster. Azimuth thruster is used so that the ASV can maneuver along curvaceous trajectory easily. This ability results in a better maneuver so that the ASV can thus minimizing contact with the barrier buoys.

D. Obstacle Field

In the Obstacle Field Task, the ASV musts circumnavigate a distinctively marked pill buoy located inside the field while avoiding the obstacle. The principle involved in this mission is similar to the one applied in the previous Obstacle Channel mission. The process starts when the ASV finds a possible opening among the obstacle buoys. This passable field would be the ASV's entry route to arrive at pill buoy. Upon arriving towards the pill buoy, the ASV would start to circumnavigate around it while avoiding obstacle buoys floating nearby. In addition to avoiding obstacle buoys, the ASV maintains a certain distance from the pill buoy by using its LiDAR sensor. Afterward, ASV would find an exit route like how it finds the entry route.

E. Acoustic Docking

The ASV executes docking and undocking maneuvers based on which beacon is active. The vehicle would identify the signal source and locate the active beacon [1]. The ASV would move at a relatively slow speed to reduce the noise caused by disturbance of the water waves generated by the propulsion and the hull. The ASV would pick up on the signal generated by the beacon using a hydrophone and process the signal to calculate the beacon location. Then the ASV would choose which Docking Bay has the active beacon.

F. Object Delivery

In this mission, the ASV is expected to deliver the objects to delivery points located at each corner of the target area. This task may be accomplished by the ASV or a combination of ASV and Unmanned Aerial Vehicle (UAV) [1].

To accomplish this mission, a UAV would assist the ASV. Using a UAV would be more advantageous to accomplish this mission because building two simple integrated systems is more simple than building a single complex ASV system to perform this task. The UAV would take off to a point where it is presumed that there exists a delivery point. The UAV would gain altitude until it detects the target drop area and then would slowly lower its altitude by following the target area. At low altitude, once the target mark is centered, the UAV would drop the object.

Afterward, the UAV would return to the coordinates where the ASV is and perform a precision landing guided by a landing mark on top of the ASV.

II. Design Creativity

In general, ASV as a system consists of several sub-systems, including hull and auxiliary structural elements, propulsion and power, Guided Navigation and Control (GNC), communication, data collection equipment, and ground station. This section will explain each critical component that we use according to the strategy described earlier.

A. Software Architecture

The Software Architecture of our ASV uses Robot Operating System (ROS) [2] as the main backbone due to its ability to make source code more reusable. The complete system consists of three (3) subsystems; ASV, UAV, and STM32. Each subsystem consists of several sensor nodes, mission planners, and actuators.

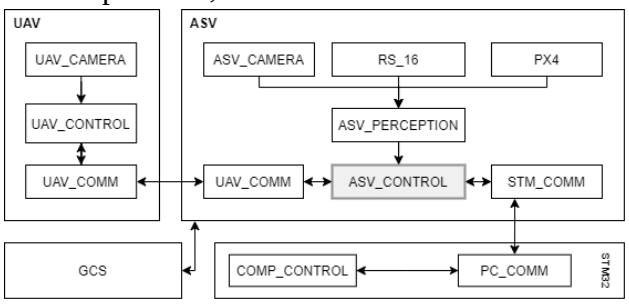

Fig. 2. Software Architecture

The ASV system consists of several sensors that are assigned to their respective sensor nodes. First, the camera sensor is assigned to the ASV_CAMERA node. This node is responsible for providing the location of an object in an image frame captured from the camera. Second, Robosense RS-16 LiDAR sensors that function for environmental sensing are assigned to RS_16 node. Lastly, the Pixhawk PX4, which handles the navigation sensors system, is assigned to MAVROS_PX4 node. This node is a Mavros ROS package that includes the mavlink communication protocol [3]. It will provide output in the form of Global Navigation Satellite System (GNSS) and Inertial Navigation System (INS) information, both in location and orientation, which is then used for guided navigation needs.

The way ASV system works starts with taking raw data from the sensor. Then, the data from the processing of sensors will be forwarded to ASV_PERCEPTION. Where in this node, the sensor data is interpreted into a perception. The perception input will read to the primary node, namely the ASV_CONTROL node. This node is in charge of controlling the ASV action based on the mission and prevailing environment. Also, it communicates with the STM32 via the STM_COMM node and UAV via the UAV_COMM node. These two nodes use the UDP protocol through RJ45 ethernet cable and Wi-Fi, respectively, because UDP provides high-speed, reliable, and real-time connection capabilities [4].

B. Guided Navigation and Control

The idea of the primary guidance of our system is divided into two (2) types, local control and global control. Local control is a guidance method using live features of objects as a reference for guidance, such as a buoy detected by a camera. On the other hand, Global Control is a guidance method using a predefined waypoint with GPS as a reference. Global Control is used when a feature object is not found. However, when ASV_PERCEPTION encounters a feature object of a task, the global control is released, and then the local control is used. The primary purpose of this system is to increase the accuracy of the control. All system guidance is entered into a PID Controller [5] to produce desired maneuvers.

Reflecting on the method used by our team in 2019, the use of headings as the primary reference for guided navigation (Global Control) between waypoints is considered less robust due to the high level of oscillation caused by noise from the

heading sensor and the harshness of the wind at the venue. Also, in several cases that were already obtained, ASV could not reach a waypoint. It only circulated at one waypoint because the desired heading control exceeds the maximum physical limit of the ASV (Fig. 3). This happened due to the error heading exceeds the control heading.

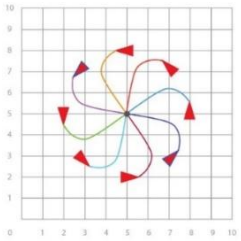

Fig. 3. Waypoint Navigation Issue

To solve this problem, the error against the waypoint is redefined from the heading error only to the combination of heading error and the perpendicular distance of ASV to the waypoint line. So, ASV is expected to maneuver, as shown in Figure 4.

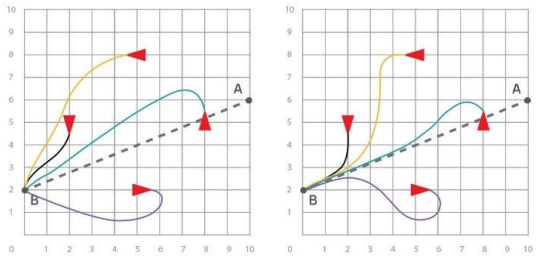

Fig. 4. The path from Waypoint A to B. Left for the 2019's algorithm, right for our proposed algorithm

C. Hull Design and Characteristic

In 2019, the hull design of the ASV was considered less stable, especially if its waves hit it. Therefore, in IRC 2021, SWATH-type was chosen to solve this problem. SWATH is a type of catamaran hull whose demi hull shapes like a cylinder beneath the water surface. It is connected to the boat deck area by a pair of thin struts. There are several advantages of using this type of hull.

Fig. 5. Proposed Roboboat Design

First, it decreases wave-making resistance. The main reason is that the SWATH struts produce relatively small waves when the ASV moves on the water. Based on the venue characteristic, this would be very beneficial. The venue, a pool, would make the resulting waves spread out to the pool's edge. These waves would later bounce off and return to the ASV, resulting in motion disturbances that could interfere with the sensor's performance (camera). Therefore, the ASV's hull must produce minor possible waves [6].

Second, it has good maneuverability and course-keeping ability. It was shown based on research that SWATH has a smaller turning radius due to the generally shorter hull length of the SWATH. In addition, there is a considerable distance between the hull and the propeller. It directs more water flow to the propeller, providing a significant turning moment even at low speed [6].

Last, it decreases motion in waves. The wave disturbances are relatively minor because most of the hull is submerged underwater, so the ASV's center of buoyancy is much lower. With proper placement of the components, the SWATH-type hull can remain stable in extreme conditions such as high waves [6]. Hence, the proposed Nala Poseidon is considered superior to the previous Nala G4, enhancing the probability of accomplishing all missions.

Stability would affect the ability of a vessel to return to its equilibrium point after receiving external forces [7]. If the ASV's stability is inadequate, it might experience several problems,

such as bad trim (tilting front and back), bad heel (tilting left and right), or capsizing. The main factor that determines the stability of the ASV is its weight distribution. The placement of the components is arranged such that the center of gravity is low. This could be achieved by placing components with a significant weight as low as possible. Proper placement of the ASV's components results in the well-trimmed ASV.

In order to do so, the placement of the components must be viewed based on three (3) reference axis, namely longitudinal (x-axis), transverse (y-axis), and vertical (z-axis).

The zero (0) point of x-axis is defined at the ASV's stern. Meanwhile, the zero (0) points of y-axis and z-axis are defined at the ASV's centerline and baseline, respectively. The components installed are batteries, ballast, laptop, and electrical system. The Maxsurf Stability software simplifies the calculation process to see the trim results due to component distribution [7].

D. ASV Perception

For the Computer Vision, a custom object detection model needs to be created to detect objects in the IRC 2021 missions. YOLOv4 architecture was used to build our custom object detection model. YOLOv4 is an improved version of YOLOv3 [8], which we used in IRC 2019.

Our custom model used transfer learning by freezing the extractor feature layer in the YOLOv4 architecture [9]. The dataset used to train the custom model has similar shapes to the COCO dataset that YOLOv4 was pretrained. Therefore, it is possible to perform transfer learning using our IRC 2021 objects dataset. With transfer learning, it is expected to increase the mean Accuracy Perfomance (mAP) level within a shorter amount of training time and a relatively small dataset on a custom model.

Fig. 6. Dataset Sample used to train the custom model

On the other hand, the object's distance can be obtained by combining the Object Detection results with LiDAR Segmentation. This can be achieved by finding the horizontal angle of an object captured by the camera that would be projected to LiDAR using (Eq. 1).

$$f(x) = \frac{diagonal_{FOV}(2x - width)}{2\sqrt{width^2 + height^2}} \qquad (1)$$

Our LiDAR Segmentation method was inspired by Morphological Transformations [10]. This process is done by converting point cloud's points to pixel points in an image. Then, OpenCV [11] Morphological Transformations is performed to the image. As a result, the neighboring pixels would merge.

E. Acoustic Signal Processing

Acoustic signal processing is a method of completing an acoustic docking mission. Our approach resembles the working system of the human ear, which likens two hydrophones to a pair of human ears. The working principle of this method is by capturing the signal from the active beacon and performing the Time Difference of Arrival (TDOA). TDOA method as the basis for processing the captured signal is chosen with some context adjustments and modifications [12], [13], [14]. The way to find the location of the acoustic signal is to estimate the angular direction received by the hydrophone. Then, the location is estimated by the accumulated angular direction of

each angular coordinate ASV. Figure 7 shows the steps to carry out the acoustic signal processing.

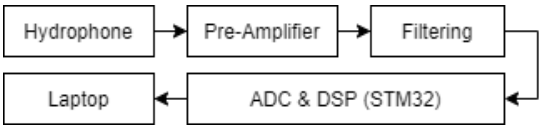

Fig. 7. Hydrophone System

First, the water conditions have to be calm and the most significant noise came from the propulsion. The estimated frequency of the noise is 1kHz, followed by echo attenuation. From these conditions, the Medium Frequency (MF) band in the range between 18-36 kHz and an accuracy of 0.25-1 m was chosen by the obtained benchmarks [13]. So, H1A Aquarian Hydrophone with frequency response between 10 Hz to 50 kHz and omnidirectional polar response capabilities was chosen [15]. The output signal from the hydrophone is processed in the PA4 pre-amplifiers [16]. Then, the Bandpass Filter (BPF) is carried out the signal frequency in the range 20-30 kHz, and there is a comparator to compare signal energy with a specified threshold.

BPF is used to minimize data noise. This identification process uses the analysis result frequency parameter. After the entire process has been passed, the desired signal target can be obtained.

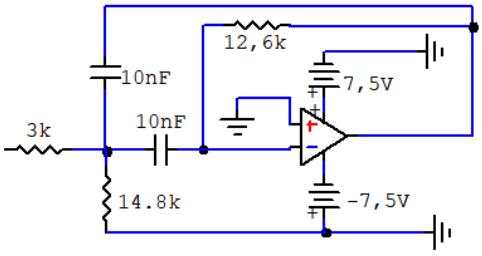

Fig. 8. Proposed Band-Pass filtering

Then, Bayesian probabilistic estimation and Markov assumption are used to obtain the probabilistic TDOA and direction angle. The angular direction of the acoustic source is obtained from the TDOA of the two hydrophones attached to the ASV. A different timestamp is required from the hydrophone with using Taylor series expansion.

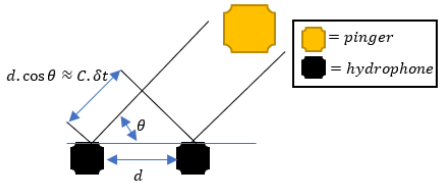

Fig. 9. Directional angle estimation of the underwater acoustic source using TDOA

$$d.\cos\theta \approx C.\delta t \quad (2)$$

Where,

C = signal velocity in the air

d = distance between 2 hydrophones

Because there are a variety of noises, estimation-based TDOA is performed using the Bayesian update process. With assumption, TDOA is determined by the time delay. Two hydrophones which has coordinates $(x_v(t-1), y_v(t-1), \theta_v(t-1))$ and $(x_v(t), y_v(t), \theta_v(t))$.

From the angular data obtained based on the coordinates of the previous stage, the accumulation of the various location directional data is used. This is due to the noise and uncertainty of the angle and position of the ASV. Thus, estimation using Unscented Kalman Filter (UKF) [17] is used over Kalman Filter [18] and Extended Kalman Filter (EKF) [19] due to system nonlinearity after comparing some of academic result [20], [21].

Since the data distance is unknown, bearings only localization is used [22], and some adjustments are added. The result of decreasing measurement data on the ASV's position and the beacon will change along with the inverse distance between beacon and ASV. Thus, the level of the estimation filter certainty with the ASV's relative position will increase. Signal processing and the calculations are done discretely with the implementation using the STM32F4 arm-based microprocessor which has ADC and several supporting peripherals [23].

F. UAV

The problem that appears with the object delivery mission was when the object is not dropped accurately on the sending platform object

due to noise on the GNSS reading sensor. To solve this problem, the UAV would be controlled based on information obtained from the camera, not from the GNSS sensor when the drone has approached setpoint object delivery.

The UAV used Pixhawk 2.1 Flight Controller. A mini-PC (Raspberry Pi 4) is attached to the UAV, acting as an onboard computing platform. The mini-PC would be responsible for image processing and controlling the UAV. A camera is also attached to the UAV to provide an image feed.

The Raspberry Pi 4 was selected as the onboard mini-PC due to its lightweight characteristics. But, Raspberry Pi 4 is limited in computational resources [24]. So, a computationally light image processing method for detecting object delivery marker and landing platform on top of the ASV is required. With that in mind, a conventional image segmentation method, HSV thresholding with morphological transformation, is implemented [10]. With the same method, the landing platform in ASV can also be detected.

G. Graphic User Interface (GUI)

Graphic User Interface (GUI) for IRC 2021 was developed using Qt. The main reason is that Qt has a framework that suits IRC 2021 mission, especially the signal and slot features [25]. The GUI helped control system parameter tuning during research and monitored the state when ASV is operating.

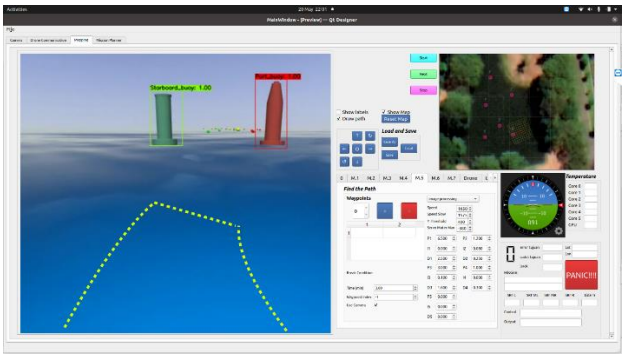

Fig. 10. ASV Software GUI

H. Simulation

For the purpose of testing our system, VRX simulation has been forked from the OSRF GitHub repository to be the base of our simulator [26]. The physics properties of the simulator were adjusted according to the characteristics of our ASV.

Fig. 11. Gazebo Simulation Message Diagram

The package THRUSTER_HANDLER was created to translate and forward control messages from ASV_CONTROL to the simulator. The simulator also publishes sensor messages such as camera image, LiDAR point clouds, INS, and GNSS, to which the ASV_PERCEPTION package would subscribe.

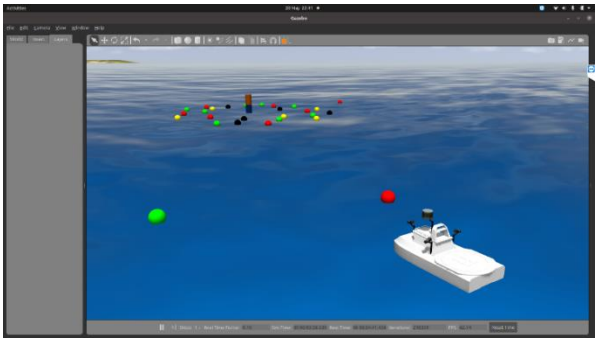

Fig. 12. Gazebo Simulation Window

III. EXPERIMENTAL RESULTS

A. Hull Performance

The 2019 IRC rule used as a reference for the principal dimensions of this year ASV, as follows:

Table 1. Principal Dimension of NALA Poseidon

Principal Dimension	
Length	100 cm
Breadth	50.4 cm
Height (Hull Only)	35 cm
Height (Total)	60 cm
Draft	17.5 cm (from baseline)
Displacement	25.61 kg

In analyzing the performance, the Nala Poseidon model is compared with the 2019 IRC ASV (Nala G4) model. This ASV performance analysis consists of two (2) major parts: resistance and seakeeping. For each simulation, each model is run at 2.4 m/s.

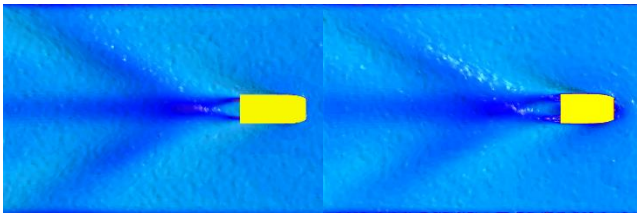

(a) (b)

Fig. 13 (a) (b) Wave Generation Pattern top view comparison between 2021 model (a) and 2019 model (b)

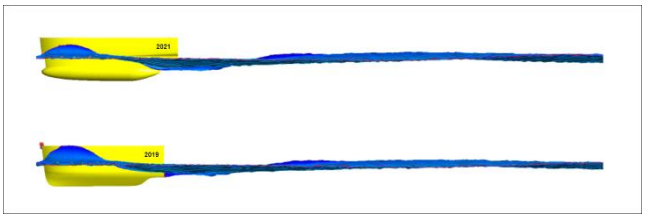

Fig. 14 Wave Generation Pattern side view comparison between 2021 model (Top) and 2019 model (Bottom)

The simulations above show that the 2021 model generated a maximum wave height of 11.33 cm. Meanwhile, the obtained maximum wave height of the 2019 model is 14.65 cm. It could be seen that the current model produces a lower maximum wave height (about 3.35 cm less) than the previous model.

The height obtained from the Computational Fluid Dynamic (CFD) analysis is used to observe the response of the vertical motion in front of the camera sensor due to the waves generated by the hull. Response of this movement can be calculated using Maxsurf Seakeeping Software by finding the Response Amplitude Operator (RAO) at a certain point on the ASV. In this simulation, the RAO is calculated for the front camera position. RAO is a function that provides the amplitude value of the oscillatory motion of the vessel due to waves acting on it [27]. Then, the data from the IRC 2019 and 2021 ASV models are compared. The following coordinates define the camera position.

Table 2. Coordinate of Camera Position

IRC Model	Longitudinal Centre [cm]	Transversal Centre [cm]	Vertical Centre [cm]
2021	82.4	0	43.5
2019	82.5	0	50.25

After the RAO is calculated, the camera sensor's vertical displacement amplitude, velocity amplitude, and acceleration amplitude can be calculated. Maxsurf Motion software is used to calculate these. For the simulation, each ASV model runs at the same speed. Meanwhile, the operating wave height value is taken from the previous CFD analysis. The final analysis result is obtained as follows:

Table 3. Final Analysis Result

Model	m0	units	RMS	Units	Significant Amplitudo		
IRC 2021	Abs. vert. motion	5.57	cm^2	2.36	cm	4.72	cm
	Abs. vert. velocity	11.89	cm^2/s^2	3.45	cm/s	6.9	cm/s
	Abs. vert. accel	227.25	cm^2/s^4	15.07	cm/s^2	30.15	cm/s^2
IRC 2019	Abs. vert. motion	13.01	cm^2	3.61	cm	7.21	cm
	Abs. vert. velocity	17.66	cm^2/s^2	4.2	cm/s	8.4	cm/s
	Abs. vert. accel	211.82	cm^2/s^4	14.55	cm/s^2	29.11	cm/s^2

The data above shows that the front camera's displacement and velocity responses of the 2021 ASV model are smaller than 2019 model. So it can be concluded that the 2021 ASV hull model is more beneficial for ASV perception sensors [28].

B. Guided Navigation Performance

Using our simulation system, the proposed algorithm and the previous algorithm were tested to obtain error data. Figure 14 below shows the progression of total error over time for the IRC 2019's GNC algorithm and the proposed GNC algorithm. The total error is defined as the root sum square of normalized heading error and perpendicular distance error. The IRC 2019's GNC algorithm's error was difficult to converge, and the error remained. Meanwhile, using the proposed GNC algorithm, the errors can converge quicker. The image shows the path generated by the two algorithms (Fig. 16). The ASV follows the

defined path closer than the previous algorithm. The previous algorithm produced a mean of total errors 0.3121, whereas the proposed algorithm produced 0.1589, half the previous algorithm.

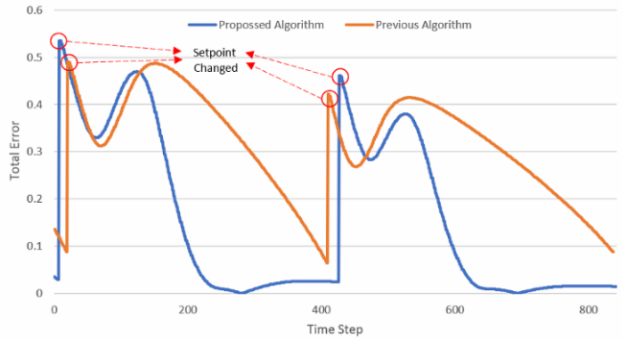

Fig. 15. Graphs Data Error

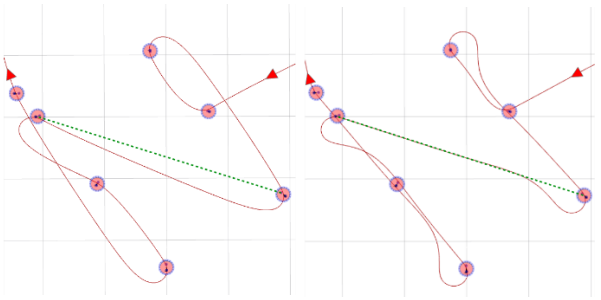

Fig. 16. Figure Path in 2019 and 2021

C. Computer Vision Performance

For the ASV, our object detection model's performance using various architectures was tested with inputs from a virtual camera provided by our gazebo simulator. These tests were ran using a Mobile Nvidia RTX 2060 6GB GPU, which would be the GPU of the PC boarded on the ASV. Table 5 below shows the comparison between the architectures. It is observed that YOLOv4 has a higher level of accuracy and bigger Frame per Second (FPS) than YOLOv3, which is better in overall performance than YOLOv3 in past competitions.

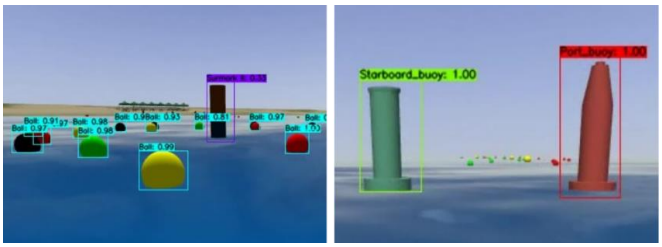

Fig. 17. Object Detection

Table 4. Performance Comparison of Yolo Models

Model	mAp	FPS	TDP
Yolo V3 (IRC 2019)	91.2	16.3	95 W
Yolo V4	92.17	29.1	95 W
Tiny Yolo V4	81.74	147.8	90 W
Tiny Yolo V4	81.74	50.6	45 W

Related distance information from objects detected by the camera is provided by the result of LiDAR segmentation. Figure 18 below shows the segmented point clouds that are limited to 10 meters radius from LiDAR.

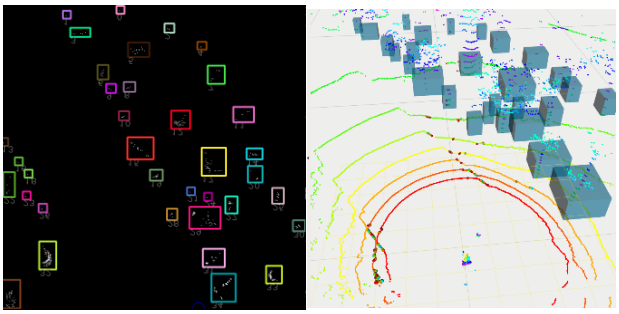

Fig. 18. Lidar 2D View and Lidar 3D View

For the UAV, the object delivery marker can be detected using the method mentioned in section II. Raspberry Pi 4 managed to obtain a solid 16 FPS.

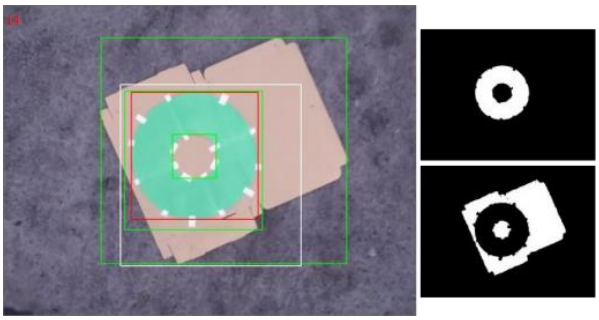

Fig. 19. UAV Computer Vision GUI

D. Acoustic Signal Processing Performance

MATLAB simulation was used to test the performance of the proposed acoustic signal processing method. After running several simulations, data in Table 5 were obtained. Distance error is defined as the Euclidean distance between the actual and estimated position. It is observed that this method can estimate the position of the active beacon with a percent relative error of 2.94%.

Table 5 Beacon location estimation

	Actual Position (x, y, z)	Estimated Position (x, y, z)	Distance Error (m)
1	(-8.098, 3.344, -4.072)	(-8.62, 3.22, -4.378)	0.61
2	(1.353, 5.479, -3.745)	(1.454, 5.82, -3.978)	0.45
3	(-7.754, -4.655, -4.673)	(-8.08, -4.83, -4.73)	0.36
4	(13.891, 8.129, 1.466)	(13.751, 8.211, 1.300)	0.39
5	(9.921, 7.22, 2.615)	(9.713, 7.01, 2.222)	0.49

IV. CONCLUSIONS

There were improvements in the overall system regarding the ASV developed from IRC 2019 to compete in IRC 2021. The new SWAT hull type is proven to have a smaller wave motion response, verified by seakeeping analysis. It is shown that there is a 34.5% decrease in the camera's vertical motion, improving the vision sensors reading. CFD analysis shows that our new hull produced a 3.32 cm lower wave height. On the other hand, to confirm the proposed GNC algorithm, we conducted a simulation using Gazebo. The simulation shows that the proposed GNC algorithm converges much faster compared to the previous algorithm. To perform object detection, YOLOv4 is utilized. A performance test shows that YOLOv4 is 44% faster and has relatively better accuracy than the YOLOv3 used in IRC 2019. Our LiDAR Segmentation method provides adequate distance information of the objects detected on the camera. HSV thresholding with morphological transformation implemented for aerial object detection provided acceptable FPS performance to perform object delivery task. The active beacon and hydrophone array system were simulated using MATLAB. With the proposed acoustic signal processing method, the beacon could be located with a percent relative error of 2.94%.

ACKNOWLEDGMENT

It is a genuine pleasure to express deep gratitude to our supervisor, philosopher, and mentor, Rudy Dikairono, MT. Without his guidance, this report would not be able to be created. We also thank all sponsors and alumni for the support so our team can participate in this competition.

REFERENCES

[1] Roboboat, “14th Annual International Roboboat Competition Rules and Task Description.” Apr. 2021.

[2] ROS, “Documentation - ROS Wiki,” *Online*. 2013, Accessed: May 22, 2021. [Online]. Available: http://wiki.ros.org/.

[3] Vladimir Ermakov, “mavros - ROS Wiki,” *ROS.org*. Accessed: May 22, 2021. [Online]. Available: http://wiki.ros.org/mavros.

[4] J. F. Kurose and K. W. Ross, *Computer Network: a top-down approach - 6th ed.* 2013.

[5] K. Ogata, *Modern Control Engineering Fifth Edition*, vol. 17, no. 3. 2009.

[6] L. Yun, A. Bliault, and H. Zong, *Catamarans and Multihulls*. 2019.

[7] M. C. Edition and M. C. Edition, “User Manual MAXSURF Stability MOSES Stability,” pp. 138–141, 2015.

[8] A. Bochkovskiy, C. Y. Wang, and H. Y. M. Liao, “YOLOv4: Optimal Speed and Accuracy of Object Detection,” *arXiv*. 2020.

[9] H. C. Shin *et al.*, “Deep Convolutional Neural Networks for Computer-Aided Detection: CNN Architectures, Dataset Characteristics and Transfer Learning,” *IEEE Trans. Med. Imaging*, vol. 35, no. 5, pp. 1285–1298, May 2016, doi: 10.1109/TMI.2016.2528162.

[10] “Computer vision: algorithms and applications,” *Choice Rev. Online*, vol. 48, no. 09, pp. 48–5140, 2011, doi: 10.5860/choice.48-5140.

[11] OpenCV, “Home - OpenCV.” 2020, Accessed: May 22, 2021. [Online]. Available: https://opencv.org/.

[12] B. Kang, J. Shin, J. Song, H. Choi, and P. Park, “Acoustic Source Localization Based on the Extended Kalman Filter for an Underwater Vehicle with a Pair of Hydrophones,” vol. 6, no. 10, pp. 641–644, 2012.

[13] P. Singh, A. Sehgal, P. Shah, and J. Kadarusman, “Autonomous underwater unmanned vehicular recovery system based on low-cost inter-aural time differentiation passive sonar,” *2007 Mediterr. Conf. Control Autom. MED*, 2007, doi: 10.1109/MED.2007.4433687.

[14] J. Choi and H. T. Choi, “Multi-target localization of

underwater acoustic sources based on probabilistic estimation of direction angle," *MTS/IEEE Ocean. 2015 - Genova Discov. Sustain. Ocean Energy a New World*, pp. 4–9, 2015, doi: 10.1109/OCEANS-Genova.2015.7271437.

[15] A. A. Products, "H2a-XLR Hydrophone User ' s Guide," *Audio*.

[16] "PA4 Datasheet," pp. 3–4.

[17] S. J. Julier and J. K. Uhlmann, "New extension of the Kalman filter to nonlinear systems," *Signal Process. Sens. Fusion, Target Recognit. VI*, vol. 3068, p. 182, 1997, doi: 10.1117/12.280797.

[18] R. E. Kalman, "A new approach to linear filtering and prediction problems," *J. Fluids Eng. Trans. ASME*, vol. 82, no. 1, pp. 35–45, 1960, doi: 10.1115/1.3662552.

[19] R. G. Brown and P. Y. . C. Hwang, "Brown R. G., Hwang P. Y. C. Introduction to random signals and applied Kalman filtering: with MATLAB exercises and solutions //Introduction to random signals and applied Kalman filtering: with MATLAB exercises and solutions, by Brown, Robert Grover.; Hwan." 1997.

[20] E. Dehghan Niri, A. Farhidzadeh, and S. Salamone, "Adaptive unscented Kalman filter (UKF) for acoustic emission (AE) source localization in noisy environment," *Heal. Monit. Struct. Biol. Syst. 2013*, vol. 8695, no. April, p. 869518, 2013, doi: 10.1117/12.2008617.

[21] W. Liu, Y. Liu, and R. Bucknall, "A Robust Localization Method for Unmanned Surface Vehicle (USV) Navigation Using Fuzzy Adaptive Kalman Filtering," *IEEE Access*, vol. 7, pp. 46071–46083, 2019, doi: 10.1109/ACCESS.2019.2909151.

[22] M. C. Deans, "Bearings-Only Localization and Mapping," pp. 1–160, 2005.

[23] "Datasheet - production data," no. STM32F47xx. 2018.

[24] Various, "Raspberry Pi 4 Model B specifications – Raspberry Pi," *Raspberry Pi Foundation*, no. BCM2711. 2020, [Online]. Available: https://www.raspberrypi.org/products/raspberry-pi-4-model-b/specifications/.

[25] T. Q. Company, "Qt | Cross-platform software development for embedded & desktop." 2017.

[26] B. Bingham *et al.*, "Toward maritime robotic simulation in gazebo," Oct. 2019, doi: 10.23919/OCEANS40490.2019.8962724.

[27] R. Bhattacharya, *Dynamics of marine vehicles*. 1978.

[28] M. C. Edition and M. C. Edition, "User Manual MAXSURF Stability MOSES Stability," 2015.

APPENDIX A : COMPONENT SPECIFICATION

See Figure A and Table A.

APPENDIX B : OUTREACH ACTIVITIES

A. *KKCTBN (National Autonomous Surface Vehicle Competition)* 2020

Fig. B. KKCTBN 2020

KKCTBN as known as Kontes Kapal Cepat Tak Berawak Nasional is the biggest national autonomous ship contest for university student in Indonesia. KKCTBN is organized by the Ministry of Education and Culture of the Republic of Indonesia. In the KKCTBN competition, three competition categories were joined by Barunastra ITS, namely ASV, ERC, and FERC. The stages of the competition include a research paper and a race competition. Barunastra ITS successfully contributed three research papers and won 1st place.

B. *RAISA* (*Robot Medical Assistant ITS*) 2020

Fig. C. RAISA 2020

RAISA is a collaborative COVID-19 patient service research robot by the Indonesian students and Barunastra ITS is part of the robot creation team.

C. I-BOAT 2020

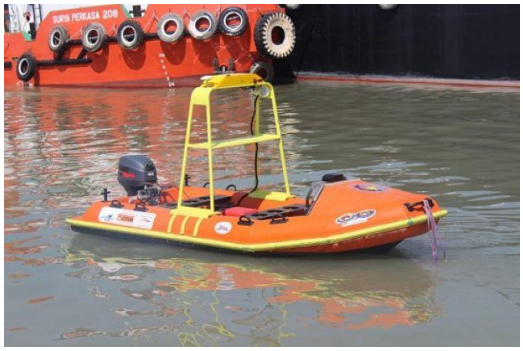

Fig. D. I-BOAT 2020

Welcoming the National Maritime Day, Barunastra ITS took part in the making of an autopilot smart ship named intelligent Boat (i-BOAT).

D. I-CAR 2020

Fig. E. I-CAR 2020

In commemoration of 75th Indonesian Independence Day Ceremony, Barunastra ITS collaborated in the newest innovation product in the form of smart electric car named intelligent Car (i-CAR).

E. INAMARINE 2019

Fig. F. INAMARINE 2019

INAMARINE is the 9th Indonesia International Shipbuilding, Offshore, Marine Equipment, Machinery & Services Exhibition 2019. It aims to accelerate the growth of the maritime industry that is being worked on by the government. Barunastra ITS showcased the NALA G4 prototype to engage the audience and raise awareness about maritime issues.

F. *IIBS (International ITS Business Summit)* 2019

Fig. G. IIBS 2019

IIBS is annual international business event held by ITS. Barunastra ITS delivered a speech about the implementation of AI systems that are applied to our boat prototype.

Fig. A. Electrical System Diagram

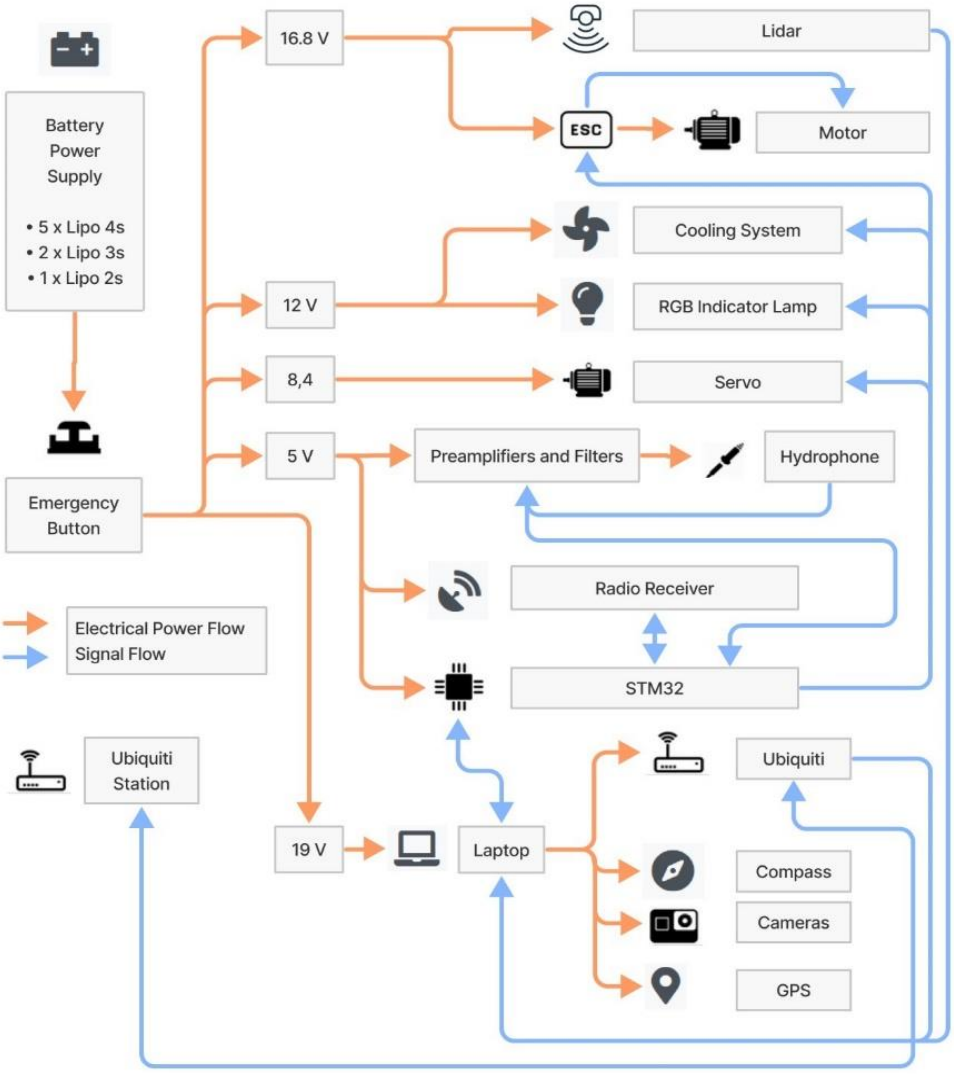

Table. A Component Specification

Components	Vendor	Model/Type	Specification	Cost
Autonomous Surface Vehicle Components				
ASV Hull	Barunastra ITS	Swath Hull	Carbon Fibre with LPP = 100 cm Breadth = 50,4 cm Height (Hull only) = 35 cm Total Height = 60 cm Draft = 17,5 cm Displacement = 25,61 kg	NN
Propulsion	Blue Robotics	T200	https://bluerobotics.com/store/thrusters/t100-t200-thrusters/t200-thruster-r2-rp/	$179.00
Propulsion System	Barunastra ITS	Azimuth Propulsion	Stainless Steel	NN
Propulsion Mover (Servo)	Savox	SC0251MG	https://www.savox-servo.com/Servos-c-1338/Brushed-Motor-c-1340/Savox-Servo-SC-0251MG-Digital-DC-Motor-Metal-Gear/	$38,85
Power System	Turnigy	Turnigy 1300mAh 2S 20C Lipo	https://hobbyking.com/en_us/turnigy-1300mah-2s-20c-lipo-pack.html	$7.24
	Onbo Power	Lipo Battery 3s 11.1v 3300mah 25-50c Onbo Nano Power	https://www.onbopower.com/m_product/469-ONBO-2200mAh-111V-80C-3S1P-FPVRacing-Dones-quads-Lipo-BatteryXT60.html	$19,98
	Onbo Power	Lipo Battery 4s 148v 6200mah 25c Onbo Nano Power	https://www.onbopower.com/m_product/138-ONBO-25C-4S-148V-6200mAh-lipo.html	$78.30
Motor Control	Blue Robotics	Basic ESC	https://bluerobotics.com/store/thrusters/speed-controllers/besc30-r3/	$27.00
CPU	MSI	GL63 8SE	https://www.msi.com/Laptop/GL63-8SX/Specification	$1,999.1
Teleoperation	Ubiquiti Network	Rocket M5	15 Km range, 350 MBps, 33 Dbm, 5.8Ghz	$124.36
INS	Pixhawk	Pixhawk2.1	http://www.proficnc.com/content/13-pixhawk2	$379.9
Camera	Logitech	C930e	https://www.logitech.com/en-us/products/webcams/c930e-business-webcam.960-000971.html	$130.00
Radio Transmitter	Futaba	10J	https://www.rc.futaba.co.jp/english/propo/air/10j.html	$399.99
Radio Receiver	Futaba	R3008SB	https://www.rc.futaba.co.jp/english/dl_manual/r3008sb_e.pdf	
Hydrophone	Aquarian Hydrophone	H1A	https://www.aquarianaudio.com/AqAudDocs/H1a_manual.pdf	$159.00
Hydrophone Preamplifier	Aquarian Hydrophone	Pa4	https://www.aquarianaudio.com/pa4.html	$94.99
LiDAR	Robosense	RS LiDAR 16	https://www.robosense.ai/en/rslidar/RS-LiDAR-16	$5,312.4
Drone System				
Aerial Vehicle Platform	Holybro	Quadcopter Frame	http://www.holybro.com/product/s500-arf-v2-frame-kit/	$88,25

Motor and Propeller	T-Motor	Air Gear 200	https://www.unmannedtechshop.co.uk/product/t-motors-air-gear-200-combo-pack/	$101,09
Power System	Onbo Power	Onbo Power 25C 4S 14.8V 3300mAh Lipo	https://www.onbopower.com/m_product/113-ONBO-25C-4S-148V-3300mAh-lipo.html	$34.66
Flight Controller	Pixhawk	Pixhawk2.1	http://www.proficnc.com/content/13-pixhawk2	$379.90
CPU	Raspberry pi	Raspberry Pi 4 Model B	https://www.raspberrypi.org/products/raspberry-pi-4-model-b/specifications/	$75.00
Telemetry	Holybro	Holybro Transceiver Telemetry V3 433 MHz	http://www.holybro.com/product/transceiver-telemetry-radio-v3/	$39.00
Camera	Raspberry pi	Raspberry Pi Cam Module V2	https://www.raspberrypi.org/products/camera-module-v2/	$25.00

Algorithm	
Algorithm	internally developed algorithms, PID Controller
Vision	OpenCV, YOLOv4
Acoustics	Band pass filtering, Preamplifiers, Bayesian rule, Markov assumption, Unscented Kalman Filter, Taylor Series Expansion, Bearings only localization, Analog to digital coverter
Localization & Mapping	Internal Development
Expertise Ratio (Hardware vs Software)	13:3
Testing Time : Simulation	1 month
Testing Time : In-water	0
Inter-Vehicle Communication	UDP, TCP, RF
Programming Language	Python 3, C++, C, MATLAB